Hulley, G.C., and S.J. Hook, 2010, Generating Consistent Land Surface Temperature and Emissivity Products Between ASTER and MODIS Data for Earth Science Research, IEEE Transactions on Geoscience and Remote Sensing, v. 49, no. 4, pp. 1304-1315, doi:10.1109/TGRS.2010.2063034.

Generating Consistent Land Surface Temperature and Emissivity (LST&E) Products Between ASTER and MODIS Data for Earth Science Research

Glynn C. Hulley and Simon J. Hook

Jet Propulsion Laboratory, California Institute of Technology, Pasadena, CA, USA

G.C. Hulley, Jet Propulsion Laboratory, 4800 Oak Grove Dr, Pasadena, CA, 91109.
glynn.hulley@jpl.nasa.gov

Abstract

Land surface temperature and emissivity (LST&E) products are generated by the Moderate Resolution Imaging Spectroradiometer (MODIS) and Advanced Spaceborne Thermal Emission and Reflection (ASTER) radiometer on NASA's Terra satellite. These products are generated at different spatial, spectral and temporal resolutions resulting in discrepancies between them that are difficult to quantify, compounded by the fact that different retrieval algorithms are used to produce them. The highest spatial resolution MODIS emissivity product currently produced is from the day/night algorithm, which has a spatial resolution of 5 km. The lack of a high spatial resolution emissivity product from MODIS limits the usefulness of the data for a variety of applications, and limits utilization with higher resolution products such as those from ASTER. This study aims to address this problem by using the ASTER Temperature

Emissivity Separation (TES) algorithm combined with an improved atmospheric correction method to generate LST&E products for MODIS at 1 km spatial resolution and for ASTER in a consistent manner. Root Mean Square (RMS) differences between ASTER and MODIS emissivities generated from TES over the southwestern USA were 0.013 at 8.6 μm and 0.0096 at 11 μm, with good correlations of up to 0.83. Validation with lab-measured sand samples from the Algodones and Kelso dunes in California showed good agreement in spectral shape and magnitude with mean emissivity differences in all bands of 0.009 and 0.010 for MODIS and ASTER respectively. These differences are equivalent to approximately 0.6 K in the LST for a material at 300 K at 11 μm.

1. INTRODUCTION

Knowledge of the land surface emissivity (LSE) is essential to derive the land surface temperature (LST), which is critical for a host of Earth surface related studies including the surface radiation budget, land use, land cover change, hydrology, and drought monitoring. High spatial resolution data (<100 m) from Landsat and the Advanced Spaceborne Thermal Emission and Reflection Radiometer (ASTER) have shown to be extremely useful in monitoring land cover and land use changes in urban [1], agricultural [2] and semi-arid areas [3]. Retrieved surface reflectance, vegetation indices and LST&E products generated from ASTER and Landsat are critical for quantifying and detecting land cover change as a result of biophysical processes. However, the full potential of these high spatial resolution sensors is often limited due to their infrequent revisit cycle of 16 days, a problem which is further compounded in cloudy regions. Conversely, the Moderate Resolution Imaging Spectroradiometer (MODIS) [4] and Atmospheric Infrared Sounder (AIRS) data [5] have high-frequency temporal resolution (twice daily) that

allows for long-term, continuous monitoring of land cover changes, but are produced at much coarser spatial resolutions of 5 km (MODIS) and 45 km (AIRS), making it difficult to quantify agricultural practices, especially in heterogeneous landscapes. Furthermore, although the LST&E products from ASTER, MODIS and AIRS represent the same measure, there are frequently discrepancies between them associated with the different scientific approaches that have been developed to derive them. Previous studies have compared the ASTER standard TES product and MODIS day/night broadband emissivities over arid regions [6] and at six SURFRAD sites [7], ASTER standard TES product and MODIS Temperature-Independent Spectral Indices (TISIE) method over a semi-arid and savannah landscape [8], and ASTER TES and MODIS day/night narrowband emissivities over the Jornado Experimental Range, New Mexico [3].

The retrieval algorithms typically used to generate LST&E products are often designed to capitalize on the unique characteristics of a given sensor, with the result that differences often exist between products that are primarily a function of the land cover type being observed. For example, the MODIS product provides accurate LST's over graybody surfaces such as dense vegetation and water, but less-accurate LST's over deserts or semi-arid regions [9], while the ASTER product provides more accurate LST's over arid regions than over graybody surfaces [10]. The algorithm inconsistency between sensors makes intercomparisons difficult to interpret, introduces uncertainties when resampling data, and limits their usefulness in models and as climate data records which require consistent and accurate LSE's over all land cover types at a range of spatial, spectral and temporal scales.

We aim to address these shortcomings and reduce the uncertainties between inter-sensor comparisons by generating LST&E products consistently from ASTER (90 m) and MODIS data (1 km) using the Temperature Emissivity Separation (TES) algorithm [11]. This could also open

up the opportunity for data fusion studies [12], by potentially generating a unified MODIS-ASTER LSE product at high spatial and temporal resolution. Recently the National Aeronautics and Space Administration (NASA) has been strongly encouraging data fusion studies for its Earth Observing System (EOS) missions in order to maximize the potential of all data on a given platform. In this paper, the output TES emissivity product from both sensors are intercompared by degrading the ASTER data product from 90 m to the MODIS spatial resolution of 1 km for mean summertime data, and then validated with lab measured field samples collected over two sand dune sites in the southwestern USA. A second intercomparison is made using a coincident ASTER-MODIS observation over the Salton Sea/Algodones dunes area on 15 June, 2000.

2. BACKGROUND

ASTER was launched on NASA's Terra satellite in December 1999, and has five spectral bands in the TIR (8-12 µm) with a spatial resolution of 90 m and repeat cycle of 16 days. The ASTER standard LST&E products (AST08 and AST05) are generated by the Temperature Emissivity Separation (TES) algorithm [11].

MODIS is a multi-spectral imager onboard the Terra and Aqua satellites of NASA's Earth Observing System (EOS), and has been the flagship for land surface remote sensing since the launch of Terra in December 1999. MODIS scans ± 55º from nadir and provides daytime and nighttime imaging of any point on the surface of the Earth every 1-2 days with a spatial resolution of ~1 km at nadir and 5 km at higher viewing angles at the scan edge [16]. MODIS LST&E standard products (MOD11 from Terra, and MYD11 from Aqua) are generated by two different algorithms: a generalized split -window (GSW) algorithm (product MOD11A1) [17]

which produces LST and two TIR longwave land classification emissivities at 1 km resolution, and a physics-based day/night algorithm (product MOD11B1) [18] which produces LST&E products at 5 km resolution for seven MODIS bands in the midwave infrared (MWIR; bands 20, 22, 23) and TIR (bands 29, 31-33).

2.1 Atmospheric Correction

The TES algorithm requires surface TIR radiance as input to generate the LST&E product. Atmospheric correction of at-sensor radiance is necessary to isolate land surface features from the effects of atmospheric emission, scattering and absorption in the Earth's atmosphere. The approach for computing surface radiance involves two steps. First, profiles of air temperature, water vapor, and geopotential height are required at the location and time of the measurement, and should be obtained from a validated, mature product with sufficient spatial resolution and close enough in time with the observation to avoid interpolation errors. And second, the atmospheric profiles are input to a radiative transfer model to compute the atmospheric parameters needed to estimate the at-surface radiance.

2.1.1 Radiative Transfer Model

The current ASTER standard atmospheric correction uses the MODTRAN 3.5 radiative transfer model [19] with input atmospheric profiles from the Global Data Assimilation System (GDAS) product provided by the National Centers for Environmental Prediction (NCEP) at 1° spatial resolution and 6-hour intervals. An interpolation scheme in both space and time is required to characterize the atmospheric conditions for an ASTER image on a pixel-by-pixel basis. This could potentially introduce large errors in air temperature and water vapor,

particularly in humid regions where atmospheric water vapor can vary on smaller spatial scales than 1°. This will propagate to errors in the atmospheric correction which in turn results in band-dependent LST&E errors in both spectral shape and magnitude.

In this study we use profiles from the MODIS joint atmospheric Level-2 product, MOD07 [20], along with an up-to-date MODTRAN 5 radiative transfer model [13] for the atmospheric correction. The latest MODTRAN version is a significant advancement over previous versions, featuring an improved molecular band model termed the Spectrally Enhanced Resolution MODTRAN (SERTRAN), resulting in much finer spectral resolution down to 0.1 cm^{-1}. The finer spectroscopy results in more accurate modeling of band absorption features in the longwave TIR window region. Other features include the treatment of auxiliary species and a rapid multi-scattering option. Validation with Line-by-Line models (LBL) have shown good accuracy.

The MOD07 product consists of profiles of temperature and moisture produced at 20 standard levels, and total precipitable water vapor (TPW), total ozone, and skin temperature produced at 5×5 MODIS 1 km pixels coincident with ASTER observations. The latest algorithm update (v5.2) includes a new improved surface emissivity training data set, with the result that RMSE differences in TPW between MOD07 and a microwave radiometer (MWR) at the Atmospheric Radiation Measurement (ARM) Southern Great Plains (SGP) site in Oklahoma were reduced from 2.9 mm to 2.5 mm [21]. Other validation campaigns have included comparisons with European Center for Medium Weather Forecasting (ECMWF) and Atmospheric Infrared Sounder (AIRS) data, radiosonde observations (RAOBS) and MWR data at ARM SGP.

2.1.2 Water Vapor Scaling (WVS) Method

Because the TES algorithm is most sensitive to uncertainties in the atmospheric correction, a Water Vapor Scaling (WVS) method is employed to further improve accuracy of the water vapor atmospheric profiles on a band-by-band basis for each observation using an Extended Multi-Channel/Water Vapor Dependent (EMC/WVD) algorithm [14]. The EMC/WVD equation models the at-surface brightness temperature, given the at-sensor brightness temperature along with an estimate of the total water vapor.

The coefficients of the EMC/WVD equations are determined using a global-based simulation model with data from the NCEP Climate Data Assimilation System (CDAS) reanalysis project. The modeled at-surface brightness temperatures are then used to compute a water vapor scaling factor that can be used to improve the atmospheric effect parameters (path radiance, transmissivity, downward sky irradiance) on a pixel-by-pixel basis. The WVS method is only applied to graybody pixels (eg. vegetation, water, some soils), and as a result an accurate gray-pixel estimation method is required prior to processing. Vegetation indices such as the Normalized Difference Vegetation Index (NDVI), land cover databases (eg. MODIS MOD12), and thermal log residuals [22] , are three different approaches that can be used in combination with each other to accomplish this. The scaling factor is then horizontally interpolated to adjacent bare pixels on the scene and smoothed before computing the improved atmospheric parameters. The interpolation should not introduce large error, since gray pixels are usually widely available in any given scene and atmospheric profiles do not change significantly at the medium-range scale (~50 km). Using 183 ASTER scenes over lakes, rivers and sea surfaces, it was found that using the WVS method instead of the standard atmospheric correction improved estimates of surface temperature from 3-8 K in regions of high humidity [14].

2.2 Temperature Emissivity Separation (TES) Algorithm

In this study the TES algorithm will be applied to both ASTER and MODIS input Level-1 B at-sensor radiances. TES is a hybridization of three independent algorithms, which together are designed to solve the ill-posed problem of separating temperature and emissivity. TES uses surface emitted TIR radiance data as input, which has been atmospherically corrected for atmospheric transmission and path radiance. The surface radiance is a combination of two terms; self emission from the Earth's surface, and reflected downward irradiance from the sky and surroundings;

$$L_{s,i} = \epsilon_i B_i(T_s) + (1 - \epsilon_i) L_i^{\downarrow} = \frac{L_i(\theta) - L_i^{\uparrow}(\theta)}{\tau_i(\theta)} \quad (1)$$

where: i - Band; θ - Viewing angle; $L_{s,i}$ - Surface radiance; ϵ_i - Surface emissivity; $B_i(T_s)$ - Planck radiance; $L_i^{\downarrow}$ - Downward sky irradiance; L_i - Observed radiance; $L_i^{\uparrow}$ - Path radiance; τ_i - Transmissivity.

The path radiance, transmissivity, and downward sky irradiance are computed with a radiative transfer model such as MODTRAN, using input atmospheric fields of temperature, relative humidity and geopotential height. The first step, called the Normalized Emissivity Method (NEM) in TES involves removing the downward sky irradiance iteratively, using an initial guess in emissivity of 0.99 (typical for most graybody surfaces). The normalized emissivities are then band ratioed relative to their means and the full emissivity spectrum can be obtained by using an empirical relationship to predict the minimum emissivity that would be observed from a given spectral contrast, or minimum-maximum emissivity difference (MMD) [23, 24]. The empirical relationship is referred to as the calibration curve and is derived from a subset of spectra from different rocks, soils, vegetation, snow, and water in the ASTER spectral library [25]. The calibration curve can be adjusted for any sensor's spectral response function in

the TIR. The ASTER and MODIS response functions along with a quartz spectrum measured from a sand sample taken from the Algodones dunes are shown in Figure 1. The 5-band ASTER TES calibration curve is given by:

$$\epsilon_{min} = 0.994 - 0.687 \cdot MMD^{0.737} \quad (2)$$

Where ϵ_{min} is the minimum emissivity of all five bands, and MMD is the difference between the minimum and maximum emissivity. Using ϵ_{min}, the full emissivity spectrum can be recovered from the emissivity band ratios, and a final LST computed by inverting the Planck function with the retrieved TES emissivities. The TES calibration curve is modified for MODIS bands 29 (8.55 μm), 31 (11 μm), and 32 (12 μm) by convolving the high resolution laboratory spectra (4 cm^{-1}) to the MODIS response functions (Figure 1). The resulting MODIS TES calibration curve for the three MODIS bands is given by:

$$\epsilon_{min} = 0.950 - 0.7503 \cdot MMD^{0.8321} \quad (3)$$

The calibration curves for ASTER (5-band) and MODIS along with the laboratory data points are shown in Figure 2. In order to demonstrate that the 3-band TES algorithm can generate accurate and consistent emissivities with MODIS data, we compute a 3-band TES algorithm for ASTER using bands 11, 13, 14 and make comparisons with the full 5-band TES algorithm to observe if consistent results are obtained. The 3-band ASTER TES calibration curve is given by:

$$\epsilon_{min} = 0.989 - 0.70 \cdot MMD^{0.749} \quad (4)$$

TES is designed to retrieve accurate emissivities of mineral substrates for applications of mineral mapping and resource exploration [11]. An ASTER validation campaign over nine sand dune sites in the southwestern USA showed that TES retrieves emissivity from remote sensing

measurements to within 0.016 for a wide range of emissivities in the TIR [10, 26]. Using field measurements at White Sands and Jornado Experimental Range in New Mexico it was also shown that TES retrieves emissivity to within 0.02 when compared to lab measurements [27]. Another advantage of TES is that is produces seamless images with no step discontinuities, as might be introduced if a land classification type algorithm was used, i.e. generalized split window algorithm. The limiting factor on TES performance is the accurate removal of atmospheric effects, specifically the estimate of atmospheric transmissivity and path radiance. Errors of more than 2 K can be expected in humid conditions if the water vapor content is not well characterized, and errors could be larger over graybody surfaces where the calibration curve is particularly sensitive to errors in atmospheric compensation [11]. These errors can be minimized using the WVS method.

3. RESULTS

3.1 Approach

The first intercomparison example in this study will compare MODIS with ASTER emissivities generated from the North American ASTER Land Surface Emissivity Database (NAALSED) v2.0 [26] on a regional scale. Version 2.0 of NAALSED uses standard ASTER products (AST05 and AST08) to generate mean, seasonal LST&E products for North America using all clear-sky ASTER scenes available from 2000-2008 (http://emissivity.jpl.nasa.gov) The current, yet to be released, version 3.0 introduces a few significant changes in that the emissivities are retrieved with an improved atmospheric correction using the methods outlined above, i.e. using MOD07 atmospheric data input to the MODTRAN 5 radiative transfer model,

and the WVS method to scale the water vapor profiles. The mean summertime (Jul-Sep, 2000-2008) NAALSED v3.0 emissivity product will be initially compared to an 8-day mean MODIS product generated from TES using data from 1-8th August 2004 over the southwestern USA. Since these two time periods are not compatible, differences in emissivity will arise in certain areas due to changes in vegetation cover and soil moisture. A second intercomparison will be made using a coincident observation over the Algodones dunes and Salton Sea area for an ASTER scene on the 15 June, 2000. For this observation, comparisons between MODIS and ASTER 3-and 5-band TES emissivity spectra results as well as differences between the WVS and standard (STD) atmospheric correction methods will be made.

For the intercomparisons, the question of how to correctly resample finer resolution emissivity data (eg. ASTER at 90 m) to coarser resolution data (eg. MODIS at 1 km) remains a challenging, and unresolved problem, and is important as it would potentially allow high spatial resolution validated data such as ASTER to be used for validating coarser resolution LSE products from MODIS (1-5 km) and AIRS (45 km) on a global scale over a wide range of different land cover types. Over homogenous areas, the effective emissivity is simply an average of finer resolution pixels that make up the scene. Writing the effective surface radiance as a sum of individual scene elements, n, we have:

$$\bar{R}_s = \bar{\varepsilon}_\nu \cdot \bar{B}_\nu(\bar{T}_s) = \frac{1}{n}\sum_{i=1}^{n} \varepsilon_{i,\nu} \cdot B_\nu(T_{i,s}) \qquad (5)$$

If each scene element is relatively constant in temperature across the scene, ie. $T_{i,s} \cong \bar{T}_s$, then the effective LSE of a scene with n elements is simply an average:

$$\bar{\varepsilon}_{\nu} = \frac{1}{n}\sum_{i=1}^{n} \varepsilon_{i,\nu} \quad (6)$$

However, over a heterogeneous scenes the problem is more complex, since the effective emissivity is dependent on different land cover components within the scene, and complicated by variations in LST, surface roughness and cavity effects, which effectively increase the emissivity at the coarser resolution [28]. Sensor spatial response function differences complicate the problem even further [29]. For heterogeneous scenes, the effective emissivity is dependent on the temperature variation within each scene element and can be written as:

$$\bar{\varepsilon}_{\nu} = \frac{1}{n}\sum_{i=1}^{n} \varepsilon_{i,\nu} \cdot B_{\nu}(T_{i,s}) \,/ \bar{B}_{\nu}(\bar{T}_{s}) \quad (7)$$

To date the scaling problem has not been investigated because the uncertainties introduced when resampling emissivity is normally masked by algorithm differences between the two sensors being compared. We will use (7) in order to resample the ASTER emissivity data (90 m) to the MODIS resolution (1 km) for the Algodones dunes observation on 15 June, 2000.

The ASTER Level-1B radiance product (AST_L1B) and MODIS radiance product (MOD021KM) are both atmospherically corrected using MODTRAN 5 with input MOD07 profiles, and the WVS method is used to improve the atmospheric parameter estimation using EMC/WVD coefficients that have been computed for each sensors' respective response functions [14, 30]. In the MODIS WVS approach, the MODIS cloud mask product (MOD35) is used for initial cloud screening [31], and the MODIS Vegetation Index Product (MOD13) combined with a new MODIS 250m water mask product, MOD44 [32] are used to classify the gray pixels on a MODIS scene. The MODIS reprojection tool is used to mosaic and geolocate these products

onto the scene of interest. For the ASTER WVS approach, the NAALSED Cloud Mask product is used for cloud screening [26, 33], and the vegetation indices (NDVI) and water mask used for gray pixel detection are computed directly from the ASTER Level-1B data [26]. Accurate cloud discrimination and gray pixel identification are two of the most important factors which determine the accuracy of the WVS method. The TES algorithm is then applied to both datasets and mean emissivities are computed using the 'stacking' method detailed in [15]. The viewing angles of MODIS are restricted to less than 30º in order to avoid non-Lambertian effects on emissivity at high view angles.

3.2 Discussion

3.2.1 Emissivity Intercomparisons

The first intercomparison example is between the NAALSED v3.0 emissivity product and a mean MODIS emissivity product computed using the TES algorithm over the study area selected over the southwestern USA. Figure 3 shows the mean emissivity results at 1 km resolution for ASTER band 11 (8.6 µm) from Jul-Sep 2000-2008, and MODIS band 29 (8.55µm) from 1-8 August 2004 which have the closest overlapping band position in the TIR region. The emissivity of ocean and inland water areas have been to set a value of 0.99, a typical value from lab-measured water spectra, using the MOD44 water mask product to identify water pixels. The bottom panels show emissivity differences (MODIS - ASTER) and a histogram of the differences excluding the water pixels. The histogram shows a positive skewness, centered at 0.01, indicating that MODIS has generally higher emissivities than ASTER over the study area. The RMSE at 8.6 µm was 0.013, which is equivalent to ~0.74 K in LST for a material at 300 K.

Figure 4 shows the comparisons for ASTER band 14 (11.3 μm) and MODIS band 31 (11 μm), which are the two closest band positions in the longwave region. Again, the MODIS LSE's are higher, with differences centered at 0.01, and an RMSE of 0.0096. Figure 5 shows a scatterplot between MODIS and ASTER emissivity at 8.6 μm for ~1.2 million pixels over the study area. There is good correlation between the two products for a wide range of emissivity values, with a R^2 value of 0.83, although differences can be as large as 0.15. For this comparison, emissivity differences between the products are algorithm independent, and result from four primary sources: surface changes, atmospheric variability, measurement error, and band position differences.

The largest emissivity differences most likely arise due to surface changes. The NAALSED v3.0 product is generated over a longer time period from 2000-2008 for the months of July-Sep, whereas the MODIS product in this study is an 8-day mean for the first week in August, 2004. As a result, the NAALSED product would most likely have lower emissivities over agricultural areas due to rotation of croplands from year-to-year. In fact, we have verified with ASTER visible data that fields may be completely bare during one year, and fully vegetated the next. Considering that on average ~5 ASTER observations are available for any given 90m pixel in NAALSED, just one low emissivity value (eg. due to bare soil) will lower the mean value by several percent. From Figure 3 it is clear that MODIS has higher emissivities by up to 0.03 over the Central Valley in CA, as well as the Imperial and Coachella valley's south and north of the Salton Sea in southwestern CA - three of the densest agricultural regions in CA. The largest LSE differences of between 0.1-0.15 can be found over the Bonneville salt flats just southwest of Great Salt Lake in northern Utah. This is a result of a higher soil moisture content over the salt flats for the MODIS observation period. Changes in surface soil moisture from

precipitation events will result in the largest differences between the two datasets for this example, as water is highly absorbing in the quartz reststrahlen band at 8.6 μm, which can result in large emissivity changes of up to 0.2 [34]. Atmospheric variability would also contribute to emissivity differences between the two products. The North American Monsoon (NAM), which manifests itself in southwestern CA and AZ during mid-July, would result in the most unpredictable changes. Even though the WVS method is used to improve the atmospheric correction for high-humidity conditions, there would still exist some residual atmospheric effects between the products as a result of the means being computed over different time periods. Lastly, since ASTER has a higher noise equivalent delta temperature (NEΔT) (0.3 K) than MODIS (0.05 K), measurement error would result in a larger apparent spectral contrast (min-max difference) with the result that emissivities are underestimated, particularly over graybody surfaces. Over geologic surfaces, variability in the TES calibration curve plays a greater role in sources of uncertainty than NEΔT [11]. Band position differences between ASTER and MODIS would also contribute to discrepancies between the products. For example, the effective wavelengths for ASTER band 11 and MODIS band 29 are integrated over different parts of the quartz reststrahlen band (see Figure 1).

The second intercomparison example uses a coincident ASTER-MODIS observation over the Algodones dunes and Salton Sea area in southeastern California on the 15 June, 2000. This area was chosen due to the heterogeneity of the land surface consisting of water, croplands, sand dunes, and mixed shrublands. Further, this observation occurred on a very humid day with MOD07 TPW greater than 3 cm, providing a stringent test for the atmospheric correction method. Since the retrieval algorithm and atmospheric correction are identical for both sensors, the only source of difference between the two products is now isolated to measurement error and

uncertainties introduced when resampling ASTER data from 90 m to the MODIS resolution of 1 km. Figure 6 shows the ASTER emissivity image for band 11 (8.6 μm) at 90 m and resampled to 1 km resolution using (7), and the MODIS emissivity image for band 29 (8.55 μm) at 1 km along with the emissivity difference (MODIS minus ASTER). White areas to the southeast of the image are due to cloud cover, and the largest differences up to 0.12 occur around this region due to undetected low-reflectance cloud in the ASTER image. Overall there is good correlation between the two images at 1 km, although the MODIS emissivities appear to be higher by 0.01-0.02 over most of the image which can be seen in the corresponding scatterplots and histograms in Figure 7. Spatially, the differences do not appear to be correlated with cover type, although over the Salton Sea and cropland areas the differences do appear to be smaller. Over bare surfaces, surface roughness and resulting cavity effects could play a part in the MODIS emissivities being higher than ASTER although this needs further investigation. For MODIS band 29 (8.55 μm) and ASTER band 11 (8.6 μm) the scatterplot has an R^2 of 0.83 and RMS of 0.019, while differences between MODIS band 31 (11 μm) and ASTER band 14 (11.3 μm) have an R^2 of 0.24 and RMS of 0.005.

3.2.2 Land Surface Temperature Intercomparisons

The land surface temperature (LSTs) retrieved from the TES algorithm for each sensor were analyzed for two areas over the Algodones dunes and Salton Sea equivalent to 1 MODIS pixel (1 km) and 10×10, 90m ASTER pixels centered at 32.97º N, 115.12ºW and 33.26º N, 115.65ºW respectively for the 15 June 2000 observation. The LST's were ~33º C for the Salton Sea and ~60º C over the Algodones dunes. The results in Table 1 show that ASTER 3-and 5-band and MODIS LST's match closely with differences of less than 1 K at both sites. The standard deviations shown are for an ASTER 10×10 pixel area over each site. Although no LST

validation data were available for this observation, the results show that the TES algorithm is able to retrieve consistent LST's irrespective of sensor or number of bands used.

3.2.3 Emissivity Validation

We have found in a previous study that large sand dune fields are particularly useful for the validation of TIR emissivity data [9]. Sand dunes have consistent and homogeneous mineralogy and physical properties over long time periods, they do not collect water for long periods as playas and pans might, and drying of the surface does not lead to cracks and fissures which could raise the emissivity due to cavity radiation effects [28]. Furthermore, the mineralogy and composition of sand samples collected in the field can be accurately determined in the laboratory using reflectance and X-Ray Diffraction (XRD) measurements. Details on the sand dune sites including temporal stability, sampling method, lab measurements, and mineralogy are described in [10] and at http://emissivity.jpl.nasa.gov/validation.

Preliminary validation of the MODIS (1-8 Aug. 2004) and the NAALSED v3.0 summertime emissivities were made with lab spectra from two sand dune sites at Algodones dunes in southwestern CA, and Kelso Dunes in the Mojave desert, which were used for validating NAALSED v2.0 [10]. Figure 8 shows emissivity spectra comparisons between MODIS and NAALSED v3.0 at Algodones dunes (top panels) and Kelso dunes (bottom panels) with lab spectra. The lab spectra at full resolution, along with the lab spectra convolved to the appropriate sensor's spectral response are shown in comparison with the MODIS and ASTER emissivity results. The lab spectra errorbars show the spatial variability in emissivity from the number of samples collected at different sites over the dunes. For Algodones dunes, there was generally good agreement with lab spectra in spectral shape for both MODIS and ASTER,

although it is interesting that both results showed lower emissivities for MODIS band 32 (12 μm), and ASTER band 14 (11.3 μm) by around 0.02. The mean absolute difference between the lab spectra and MODIS data was 0.0095 and between the lab spectra and ASTER data was 0.011 for all bands. For Kelso dunes, the MODIS and ASTER emissivities were slightly higher in all bands by approximately 0.01, although both MODIS and ASTER capture the spectral shape very well. Mean absolute differences this time were 0.011 for MODIS and 0.012 for ASTER. The reasons for the higher emissivities in this case could be that Kelso dunes are covered by a small fraction of dune reed grass in some areas, which would increase the emissivity from the remote sensing point of view.

In order to check the validity of the MODIS 3-band TES algorithm, we ran TES for the Algodones observation on the 15 June 2000 using an ASTER 3-and 5-band calibration curves given by (2) and (4) to see if any apparent differences could be observed from the results. The results in Figure 9 over the Algodones dunes show that the emissivities retrieved by both ASTER calibration curves are almost identical with negligible differences, which demonstrates that the 3-band TES algorithm is able to retrieve accurate emissivities in magnitude and spectral shape and is therefore valid for MODIS data. The MODIS and ASTER data compare well with the lab measurements for this observation, although again we see lower emissivities by 0.02 for the longest wavelength (at 12 μm for MODIS, and 11.3 μm for ASTER) compared to the lab results.

Lastly, we looked at emissivity spectra over the Salton Sea to observe what effects applying the WVS atmospheric correction method had on the shape of the emissivity spectrum when compared to using the standard correction (STD). The emissivity spectrum of water is high (~0.98) and flat and the results in Figure 10 show a dramatic improvement in emissivity accuracy in both magnitude (up to 0.06 for ASTER band 11, and 0.09 for MODIS band 29) and spectral

shape when using WVS as opposed to STD method. Because of the humid day, where MOD07 PWV values were around 4 cm over the water, the spectral contrast of the STD emissivity results are overestimated for ASTER and MODIS data. However, when applying the WVS method, the ASTER emissivity spectra fall within 0.015 of the lab measured spectrum while MODIS emissivity spectra are within 0.005 at all wavelengths. Again, differences between the 3-and 5-band TES algorithm applied to ASTER data were small.

4. CONCLUSIONS

The goal of this study was to generate consistent land surface temperature and emissivity (LST&E) products between ASTER and MODIS using the Temperature Emissivity Separation (TES) algorithm. This method eliminates discrepancies between current LST&E products produced from these two sensors which arise primarily from different scientific methods that are used to produce them. Furthermore, the MODIS TES product will be produced at a higher spatial resolution (1 km) than current MOD11 emissivity products which are produced at 5 km resolution. Producing a 1 km, twice-daily, MODIS emissivity dataset would be ideal for quantifying and monitoring cropland phenology for example. Individual fields could be isolated, and distinct phenology changes due to planting and harvesting schedules, along with high frequency natural events from precipitation, and changes in soil moisture could be monitored at high spatial and temporal resolution.

Emissivity intercomparisons between the MODIS TES and NAALSED v3.0 product over the western USA showed good agreement for ASTER band 11 (8.6 μm) and MODIS band 29 (8.55 μm) with a RMSE of 0.013 and R^2 of 0.83. Further comparisons were made for ASTER

band 14 (11.3 μm) and MODIS band 31 (11 μm), and in this case the RMSE was 0.0096. For both band positions, the MODIS emissivities were on average 0.01 higher than ASTER. Since the mean NAALSED product is produced over a longer time period (Jul-Aug, 2000-2008) than the MODIS data used in this study (8-day, July 2004), differences between the two products arose primarily due to surface changes in vegetation and soil moisture, which resulted in differences of more than 0.15 in emissivity over certain areas. Atmospheric variability, and sensor dependent characteristics such as measurement error (NEΔT) and band positions would contribute to emissivity differences to a lesser extent. A second comparison using a coincident ASTER-MODIS observation over the Algodones dunes on 15 June 2000 showed similar results, with a RMSE of 0.019 and R^2 of 0.83 for ASTER band 11 (8.6 μm) and MODIS band 29 (8.55 μm), and a RMSE of 0.005 and R^2 of 0.24 for ASTER band 14 (11.3 μm) and MODIS band 31 (11 μm).

A preliminary validation was performed with lab-measured sand samples from the Algodones dunes and Kelso dunes in CA. Both MODIS and ASTER captured the spectral shape of these two dune sites very well, with mean absolute differences in all bands of 0.0095 and 0.011 respectively. Comparisons between a 3-and 5-band TES algorithm applied to ASTER data showed negligible differences over bare and water surfaces, and we showed that applying the WVS method during humid conditions significantly improved the emissivity accuracy in both magnitude (from 0.06-0.09) and spectral shape when compared to the standard atmospheric correction method.

The synergy of multi-sensor and multi-platform products is essential for laying down a baseline quality metric to which future climate datasets and trends can be measured, and generating consistent products with the same algorithm will open up the opportunity for

producing a unified MODIS-ASTER emissivity product that can be used by the broad scientific community to provide accurate land surface temperatures and other products in a consistent manner at multiple temporal, spatial and spectral scales.

Acknowledgements

The research described in this paper was carried out at the Jet Propulsion Laboratory, California Institute of Technology, under the contract with the National Aeronautics and Space Administration. ASTER data was provided by NASA/GSFC/METI/ERSDAC/JAROS, and U.S./Japan ASTER Science Team.

References

1 Stefanov, W.L., Ramsey, M.S., and Christensen, P.R.: 'Monitoring urban land cover change: An expert system approach to land cover classification of semiarid to arid urban centers', *Remote Sensing of Environment*, 77, (2), pp. 173-185, 2001

2 Liu, J.Y., Liu, M.L., Tian, H.Q., Zhuang, D.F., Zhang, Z.X., Zhang, W., Tang, X.M., and Deng, X.Z.: 'Spatial and temporal patterns of China's cropland during 1990-2000: An analysis based on Landsat TM data', *Remote Sensing of Environment*, 98, (4), pp. 442-456, 2005

3 French, A.N., Schmugge, T.J., Ritchie, J.C., Hsu, A., Jacob, F., and Ogawa, K.: 'Detecting land cover change at the Jornada Experimental Range, New Mexico with ASTER emissivities', *Remote Sensing of Environment*, 112, (4), pp. 1730-1748, 2008

4 Justice, C.O., Vermote, E., Townshend, J.R.G., Defries, R., Roy, D.P., Hall, D.K., Salomonson, V.V., Privette, J.L., Riggs, G., Strahler, A., Lucht, W., Myneni, R.B., Knyazikhin, Y., Running, S.W., Nemani, R.R., Wan, Z.M., Huete, A.R., van Leeuwen, W., Wolfe, R.E., Giglio, L., Muller, J.P., Lewis, P., and Barnsley, M.J.: 'The Moderate Resolution Imaging Spectroradiometer (MODIS): Land remote sensing for global change research', *Ieee Transactions on Geoscience and Remote Sensing*, 36, (4), pp. 1228-1249, 1998

5 Zhou, L., Goldberg, M., Barnet, C., Cheng, Z., Sun, F., Wolf, W., King, T., Liu, X., Sun, H., and Divakarla, M.: 'Regressioin of surface spectral emissivity from hyperspectural instruments', *Ieee Transactions on Geoscience and Remote Sensing*, 46, (2), pp. 328-333, 2008

6 Ogawa, K., Schmugge, T., and Rokugawa, S.: 'Estimating broadband emissivity of arid regions and its seasonal variations using thermal infrared remote sensing', *Ieee Transactions on Geoscience and Remote Sensing*, 46, (2), pp. 334-343, 2008
7 Wang, K.C., and Liang, S.L.: 'Evaluation of ASTER and MODIS land surface temperature and emissivity products using long-term surface longwave radiation observations at SURFRAD sites', *Remote Sensing of Environment*, 113, (7), pp. 1556-1565, 2009
8 Jacob, F., Petitcolin, F., Schmugge, T., Vermote, E., French, A., and Ogawa, K.: 'Comparison of land surface emissivity and radiometric temperature derived from MODIS and ASTER sensors', *Remote Sensing of Environment*, 90, (2), pp. 137-152, 2004
9 Hulley, G.C., and Hook, S.J.: 'Intercomparison of Versions 4, 4.1 and 5 of the MODIS Land Surface Temperature and Emissivity Products and Validation with Laboratory Measurements of Sand Samples from the Namib Desert, Namibia', *Remote Sensing of Environment*, 113, pp. 1313-1318, 2009
10 Hulley, G.C., Hook, S.J., and Baldridge, A.M.: 'Validation of the North American ASTER Land Surface Emissivity Database (NAALSED) Version 2.0 using Pseudo-Invariant Sand Dune Sites', *Remote Sensing of Environment*, 113, pp. 2224-2233, 2009
11 Gillespie, A., Rokugawa, S., Matsunaga, T., Cothern, J.S., Hook, S., and Kahle, A.B.: 'A temperature and emissivity separation algorithm for Advanced Spaceborne Thermal Emission and Reflection Radiometer (ASTER) images', *IEEE Transactions on Geoscience and Remote Sensing*, 36, (4), pp. 1113-1126, 1998
12 Gao, F., Masek, J., Schwaller, M., and Hall, F.: 'On the blending of the Landsat and MODIS surface reflectance: Predicting daily Landsat surface reflectance', *Ieee Transactions on Geoscience and Remote Sensing*, 44, (8), pp. 2207-2218, 2006
13 Berk, A., Anderson, G.P., Acharya, P.K., Bernstein, L.S., Muratov, L., Lee, J., FOx, M., Adler-Golden, S.M., Chetwynd, J.H., Hoke, M.L., Lockwood, R.B., Gardner, J.A., Cooley, T.W., Borel, C.C., and Lewis, P.E.: 'MODTRAN^{TM} 5, A Reformulated Atmospheric Band Model with Auxiliary Species and Practical Multiple Scattering Options: Update'. Algorithms and Technologies for Multispectral, Hyperspectral, and Ultraspectral Imagery XI, Bellingham, WA, 2005
14 Tonooka, H.: 'Accurate atmospheric correction of ASTER thermal infrared imagery using the WVS method', *Ieee Transactions on Geoscience and Remote Sensing*, 43, (12), pp. 2778-2792, 2005
15 Hulley, G.C., Hook, S.J., and Baldridge, A.M.: 'ASTER land surface emissivity database of California and Nevada', *Geophysical Research Letters*, 35, (13), pp. L13401, doi: 13410.11029/12008gl034507, 2008
16 Wolfe, R.E., Roy, D.P., and Vermote, E.: 'MODIS land data storage, gridding, and compositing methodology: Level 2 grid', *Ieee Transactions on Geoscience and Remote Sensing*, 36, (4), pp. 1324-1338, 1998
17 Wan, Z.M., and Dozier, J.: 'A generalized split-window algorithm for retrieving land-surface temperature from space', *IEEE Transactions on Geoscience and Remote Sensing*, 34, (4), pp. 892-905, 1996
18 Wan, Z.M., and Li, Z.L.: 'A physics-based algorithm for retrieving land-surface emissivity and temperature from EOS/MODIS data', *Ieee Transactions on Geoscience and Remote Sensing*, 35, (4), pp. 980-996, 1997
19 Kneizys, F.X., Abreu, L.W., Anderson, G.P., Chetwynd, J.H., Shettle, E.P., Berk, A., Bernstein, L.S., Robertson, D.C., Acharya, P.K., Rothman, L.A., Selby, J.E.A., Gallery, W.O.,

and Clough, S.A.: 'The MODTRAN 2/3 Report & LOWTRAN 7 Model, F19628-91-C-0132'. Phillips Lab, Hanscom AFB, MA, 1996
20 Seemann, S.W., Li, J., Menzel, W.P., and Gumley, L.E.: 'Operational retrieval of atmospheric temperature, moisture, and ozone from MODIS infrared radiances', *Journal of Applied Meteorology*, 42, (8), pp. 1072-1091, 2003
21 Seemann, S.W., Borbas, E.E., Knuteson, R.O., Stephenson, G.R., and Huang, H.L.: 'Development of a global infrared land surface emissivity database for application to clear sky sounding retrievals from multispectral satellite radiance measurements', *Journal of Applied Meteorology and Climatology*, 47, (1), pp. 108-123, 2008
22 Hook, S.J., Gabell, A.R., Green, A.A., and Kealy, P.S.: 'A Comparison of Techniques for Extracting Emissivity Information from Thermal Infrared Data for Geologic Studies', *Remote Sensing of Environment*, 42, (2), pp. 123-135, 1992
23 Kealy, P.S., and Hook, S.: 'Separating temperature & emissivity in thermal infrared multispectral scanner data: Implication for recovering land surface temperatures.', *IEEE Transactions on Geoscience and Remote Sensing*, 31, (6), pp. 1155-1164, 1993
24 Matsunaga, T.: 'A temperature-emissivity separation method using an empirical relationship between the mean, the maximum, & the minimum of the thermal infrared emissivity spectrum, in Japanese with English abstract.', *Journal Remote Sensing Society Japan*, 14, (2), pp. 230-241, 1994
25 Baldridge, A.M., Hook, S.J., Grove, C.I., and Rivera, G.: 'The ASTER Spectral Library Version 2.0', *Remote Sensing of Environment*, 114, (4), pp. 711-715, 2009
26 Hulley, G.C., and Hook, S.J.: 'The North American ASTER Land Surface Emissivity Database (NAALSED) Version 2.0', *Remote Sensing of Environment*, (113), pp. 1967-1975, 2009
27 Mira, M., Schmugge, T., Valor, E., Caselles, V., and Coll, C.: 'Comparison of Thermal Infrared Emissivities Retrieved With the Two-Lid Box and the TES Methods With Laboratory Spectra', *Ieee Transactions on Geoscience and Remote Sensing*, 47, (4), pp. 1012-1021, 2009
28 Mushkin, A., and Gillespie, A.R.: 'Estimating sub-pixel surface roughness using remotely sensed stereoscopic data', *Remote Sensing of Environment*, 99, (1-2), pp. 75-83, 2005
29 Schreier, M.M., Kahn, B.H., Eldering, A., Elliot, D.A., Fishbein, E., Irion, F.W., and Pagano, T.S.: 'Radiance Comparisons of MODIS and AIRS using spatial response information', *J. Atmos. Ocean. Tech.*, pp. in press., 2010
30 Tonooka, H.: 'Atmospheric Correction of MODIS Thermal Infrared Bands by Water Vapor Scaling Method', in Editor (Ed.)^(Eds.): 'Book Atmospheric Correction of MODIS Thermal Infrared Bands by Water Vapor Scaling Method' (2005, edn.), pp. 152-163
31 Ackerman, S.A., Strabala, K.I., Menzel, W.P., Frey, R.A., Moeller, C.C., and Gumley, L.E.: 'Discriminating clear sky from clouds with MODIS', *Journal of Geophysical Research-Atmospheres*, 103, (D24), pp. 32141-32157, 1998
32 Carroll, M.L., Townshend, J.R., DiMiceli, C.M., Noojipady, P., and Sohlberg, R.A.: 'A new global raster water mask at 250 m resolution', *International Journal of Digital Earth*, 2, (4), pp. 291-308, 2009
33 Hulley, G.C., and Hook, S.J.: 'A new methodology for cloud detection and classification with ASTER data', *Geophysical Research Letters*, 35, (16), pp. L16812, doi: 16810.11029/12008gl034644, 2008

34 Mira, M., Valor, E., Boluda, R., Caselles, V., and Coll, C.: 'Influence of soil water content on the thermal infrared emissivity of bare soils: Implication for land surface temperature determination', *Journal of Geophysical Research-Earth Surface*, 112, (F4), pp. F04003, 2007

Table 1. Surface temperature comparisons between ASTER (3-band), ASTER (5-band) and MODIS using the TES algorithm at Algodones dunes and Salton Sea on 15 June, 2000. Standard deviations for ASTER are for a 10×10, 90m pixel area corresponding to one MODIS 1 km pixel. Differences between the three methods at both sites are <1 K.

	ASTER (5-band)	ASTER (3-band)	MODIS
Algodones dunes	333.9 ± 0.6	334.2 ± 0.6	334.5
Salton Sea	306.3 ± 0.3	306.7 ± 0.3	307.2

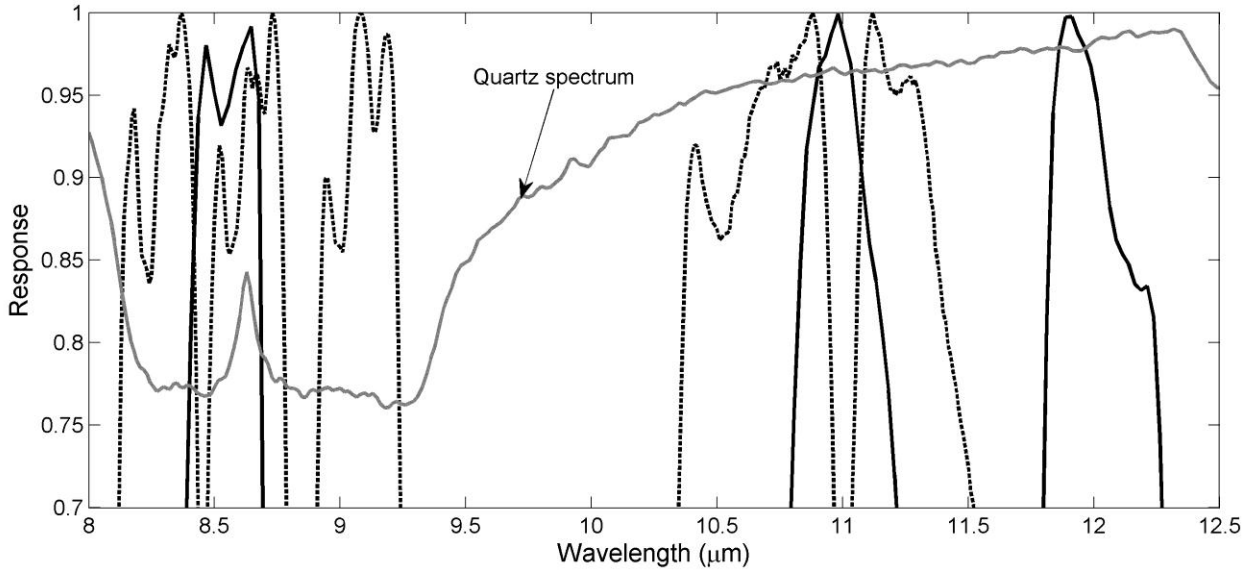

Figure 1. Spectral response functions for MODIS bands 29, 31, 32 (black solid) and ASTER bands 10-14 (black dashed) in the TIR region (8-13 μm). Also shown is a quartz spectrum measured from a sand sample taken from the Algodones dunes, CA (gray solid).

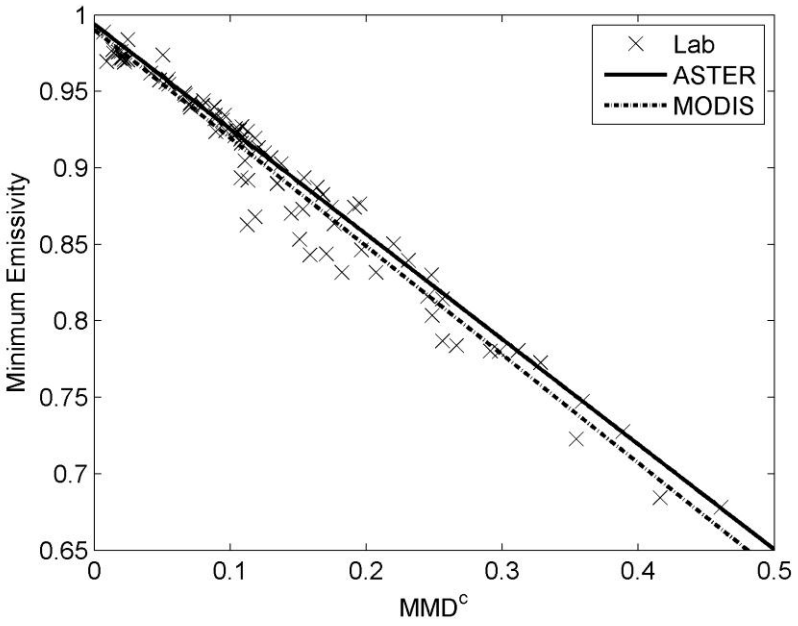

Figure 2. ASTER and MODIS calibration curves of minimum emissivity vs min-max difference (MMD), where c is the coefficient for MODIS (0.8321) and ASTER (0.737). The lab data (crosses) are computed from more than 90 spectra consisting of a broad range of terrestrial materials (rocks, sand, soil, water, vegetation, ice).

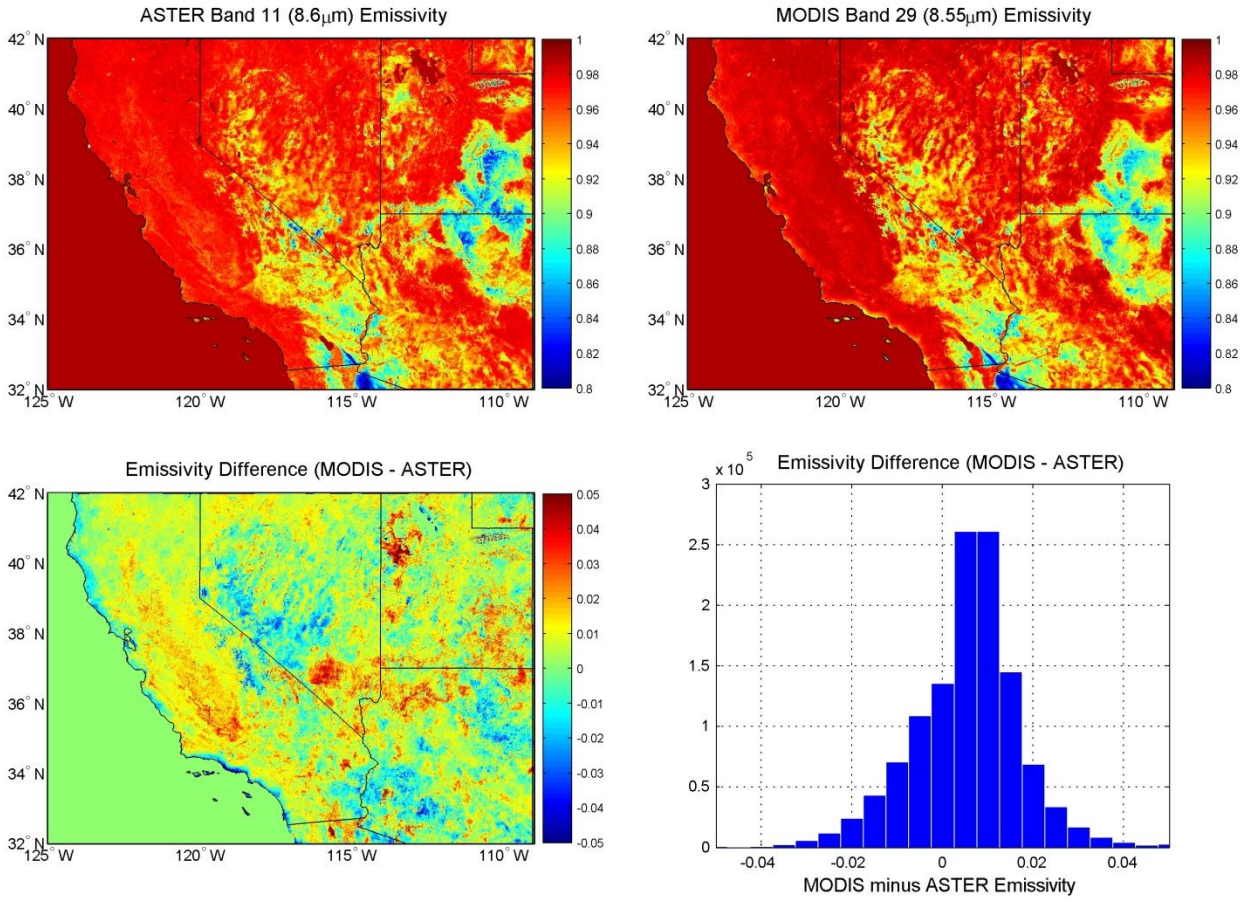

Figure 3. Mean emissivity images retrieved using the TES algorithm for ASTER band 11 (8.6 μm) for July-September 2000-2009, and for MODIS band 29 (8.55 μm) from 1-8 August 2004 over the southwestern USA at 1 km spatial resolution.

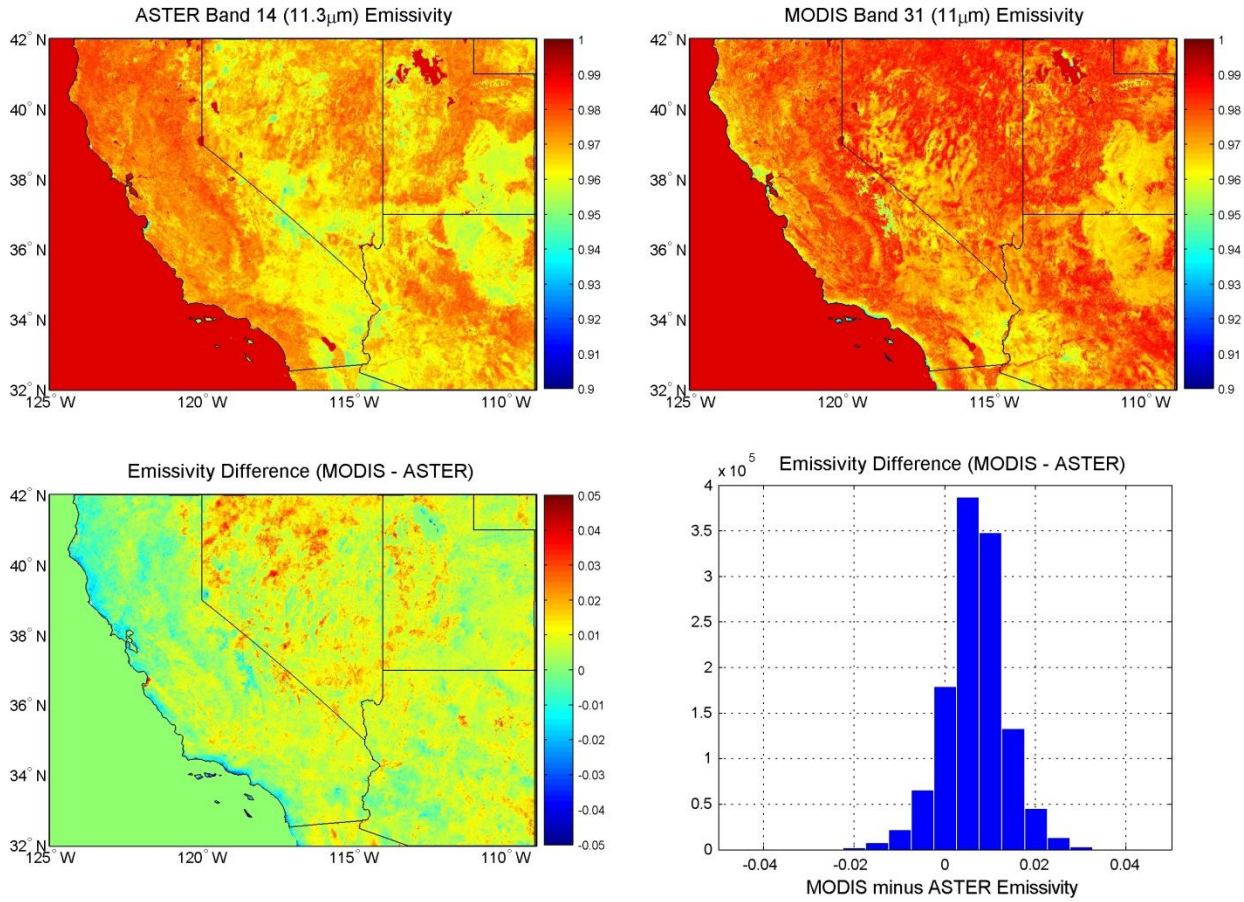

Figure 4. Mean emissivity images retrieved using the TES algorithm for ASTER band 14 (11.3 μm) for July-September 2000-2009, and for MODIS band 31 (11 μm) from 1-8 August 2004 over the southwestern USA at 1 km spatial resolution.

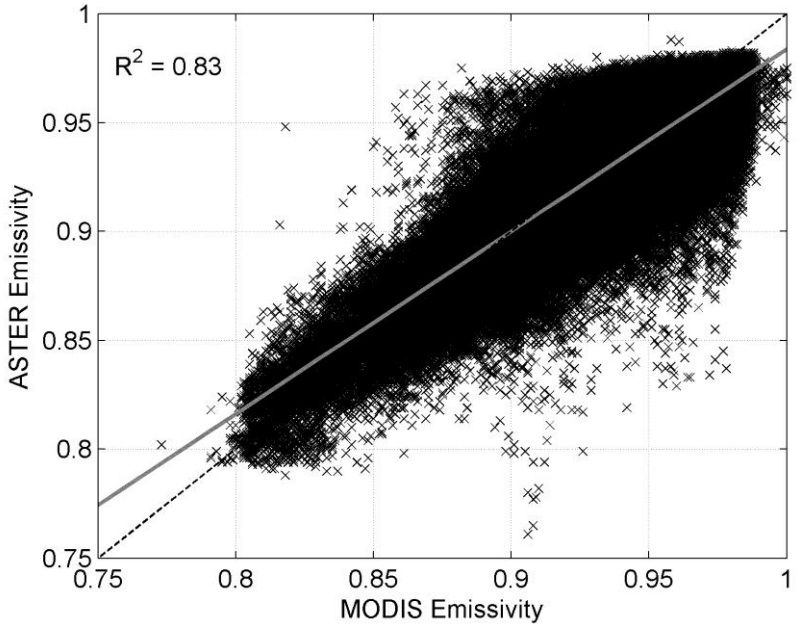

Figure 5. Scatterplot of ASTER vs MODIS emissivity at 8.6 μm for ~1.2 million 1 km pixels over the southwestern USA. Crosses show the emissivity data points, dashed line shows 1-to-1 line, and solid gray line shows the best fit line through the data.

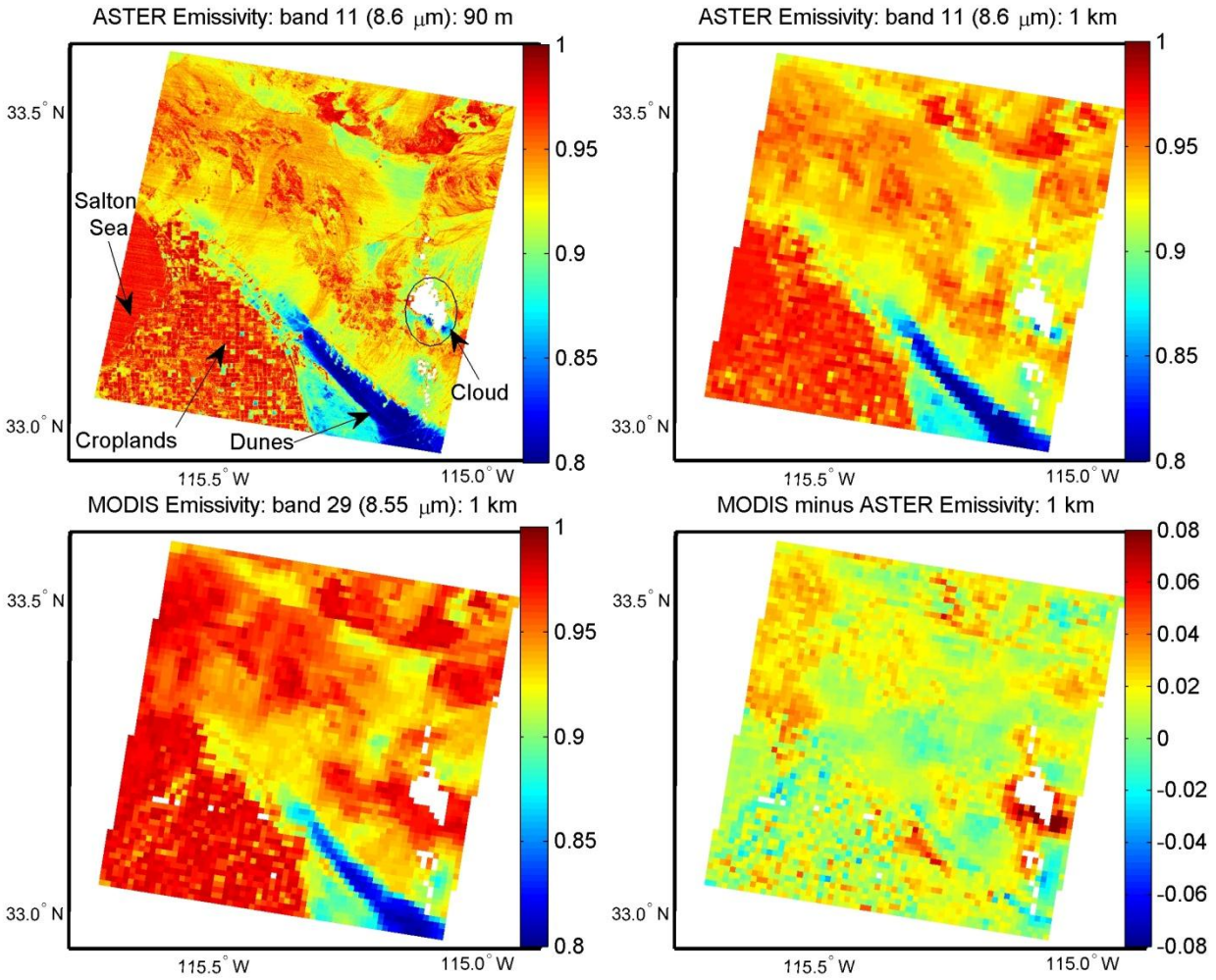

Figure 6. Emissivity images of ASTER band 11 (8.6 µm) at 90 m, ASTER band 11 (8.6 µm) resampled to 1 km, MODIS band 29 (8.55 µm) at 1 km, and MODIS minus ASTER emissivity at 1km.

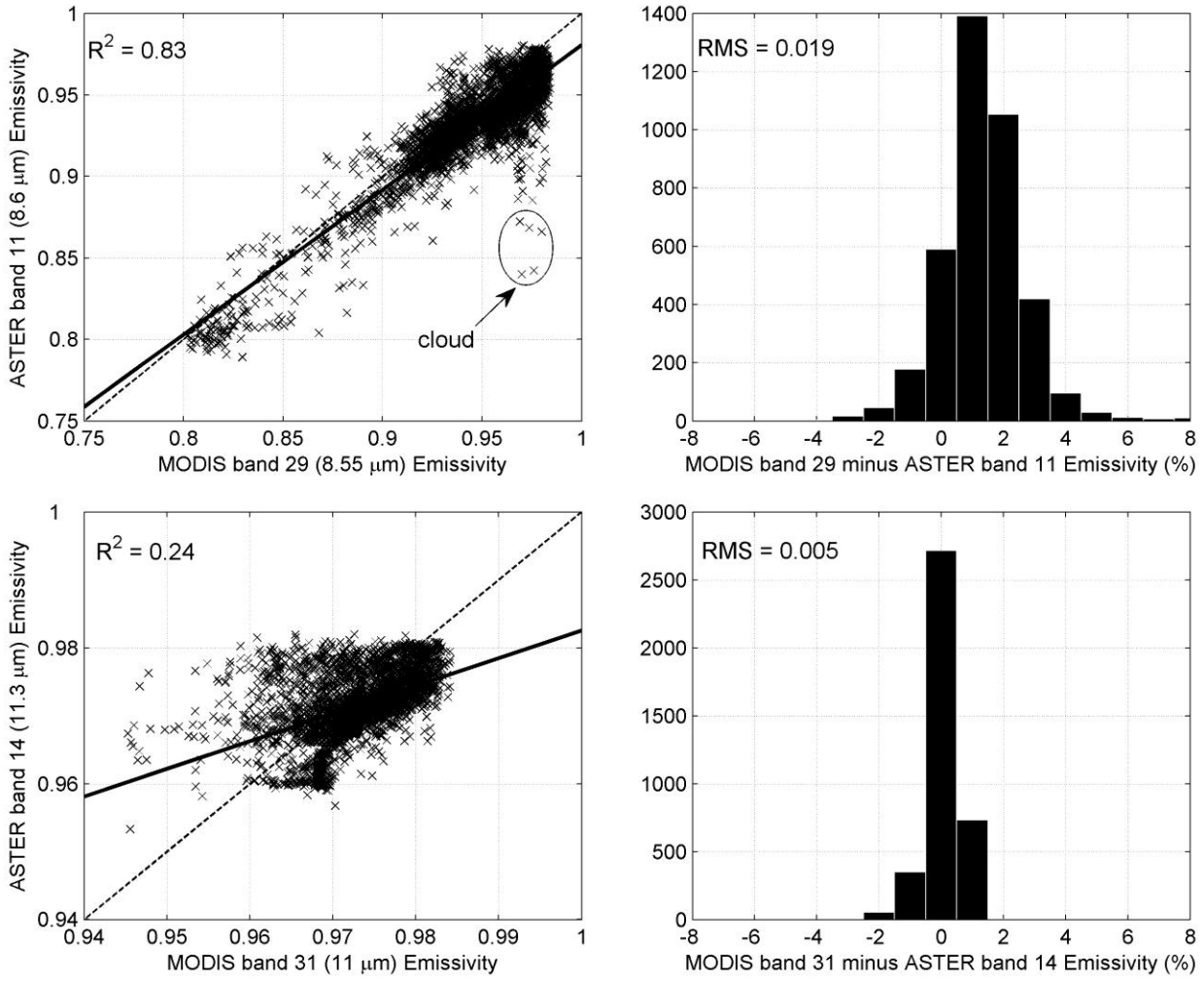

Figure 7. Emissivity scatterplots (left) and histograms (right) of MODIS and ASTER retrieved emissivities for the observation on 15 June 2000. Note the low ASTER emissivities in band 11 due to low-reflective cloud contamination in the ASTER image.

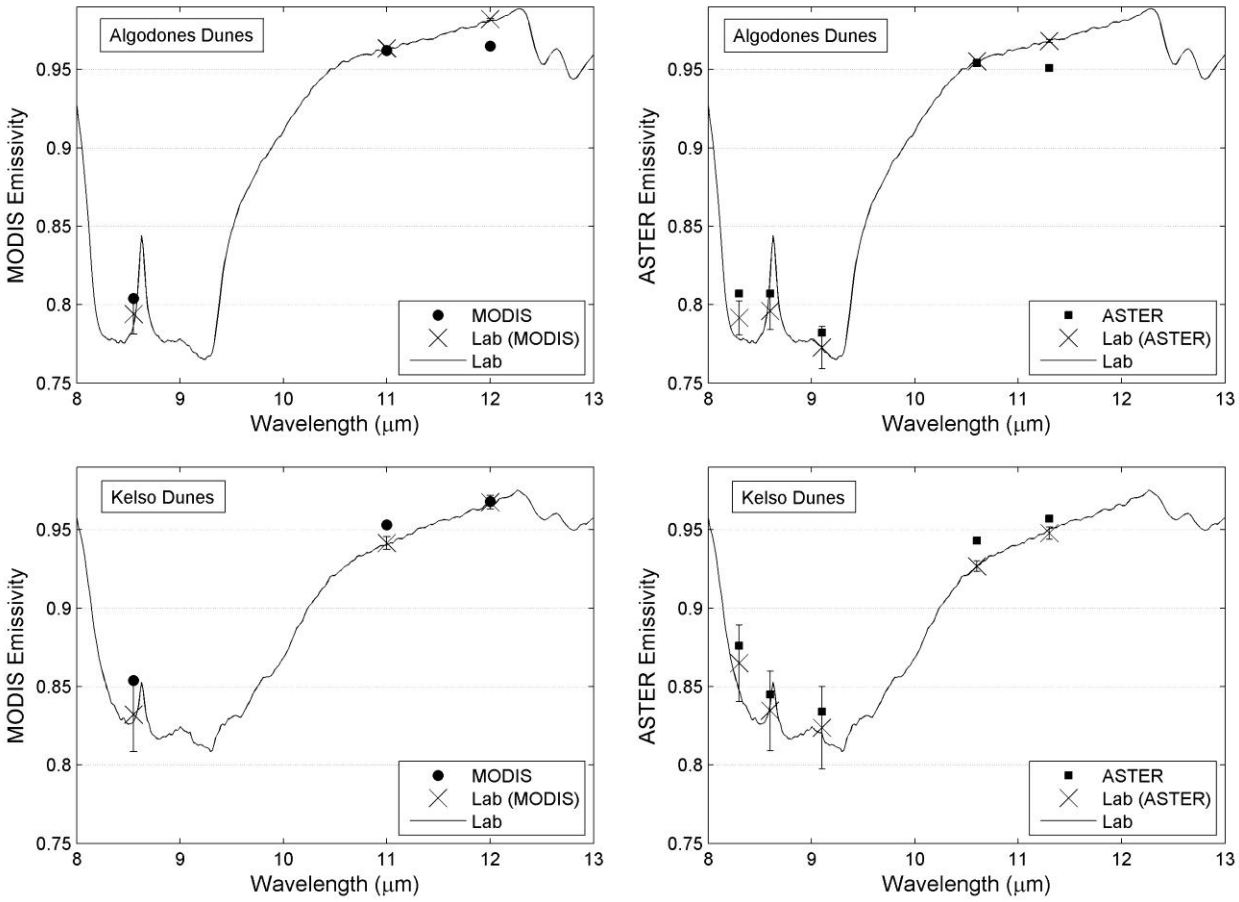

Figure 8. Emissivity spectra comparisons between MODIS (left) and ASTER (right) and lab-measured sand samples collected at Algodones dunes (top) and Kelso dunes (bottom) validation sites in California. Crosses show the lab spectra convolved to the appropriate sensor's spectral response function (see Figure 1).

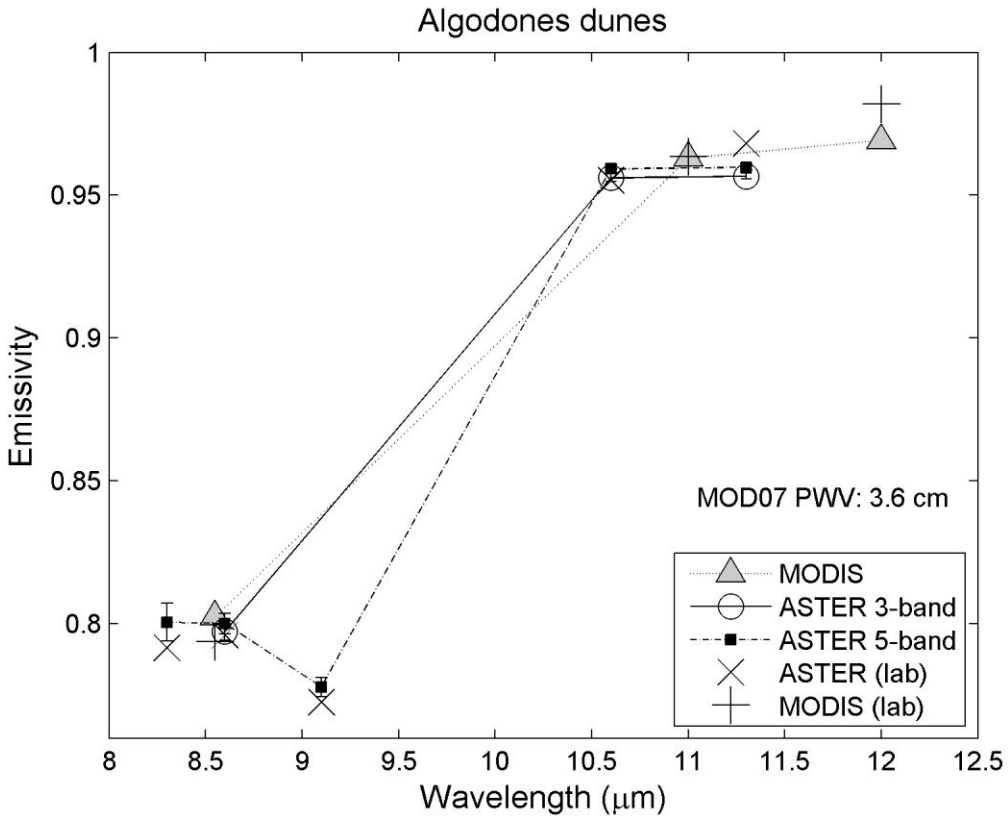

Figure 9. Emissivity spectra comparisons at the Algodones dunes on 15 June 2000 between MODIS, ASTER (3-band), ASTER (5-band), and lab measurements convolved to the appropriate sensor's response function (crosses and plus signs). The TES algorithm and Water Vapor Scaling (WVS) method were used for the retrievals. Also shown is an estimate of the precipitable water vapor (PWV) from the MOD07 atmospheric product.

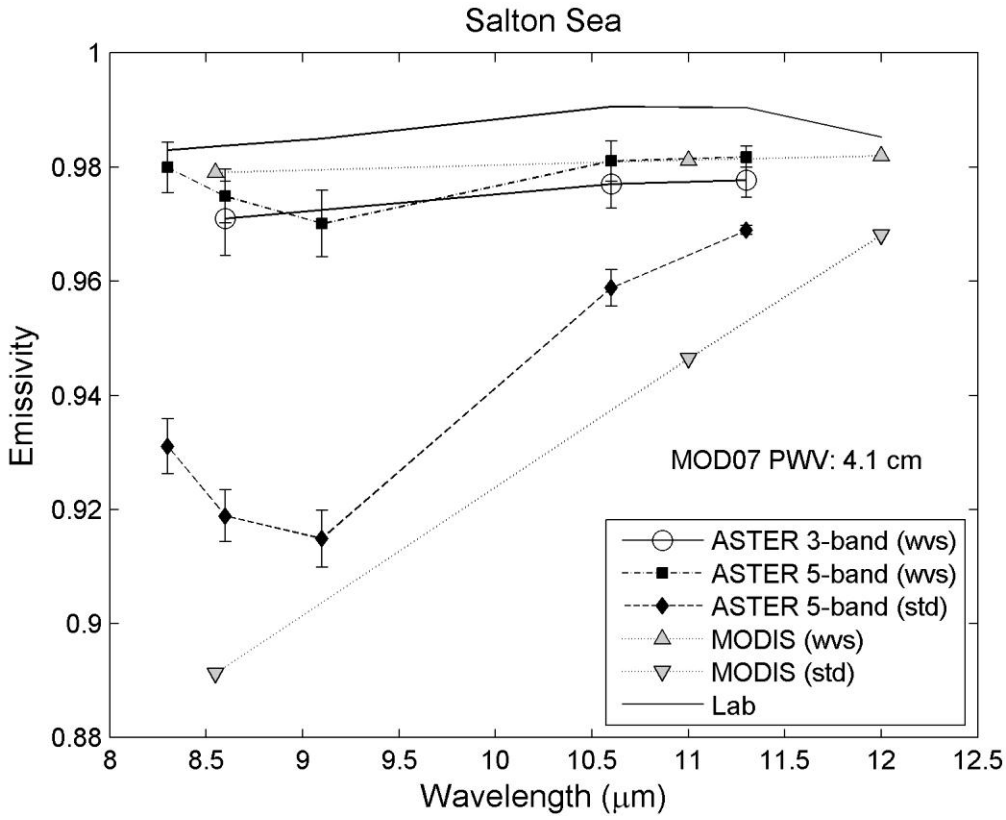

Figure 10. Emissivity spectra comparisons for the Salton Sea on 15 June 2000 between ASTER (3-band), ASTER (5-band) and MODIS using the TES algorithm, along with lab spectra of water from the ASTER spectral library. Results from the Water Vapor Scaling (wvs) method and the standard (std) atmospheric correction are also shown. An estimate of the precipitable water vapor (PWV) from the MOD07 atmospheric product indicates very high humidity on this day.